

AIAA 80-0156R

Transonic Flow Calculations for a Wing in a Wind Tunnel

J. E. Mercer,* E. W. Geller,* and M. L. Johnson†

Flow Research Company, Kent, Wash.

and

A. Jameson‡

Princeton University, Princeton, N. J.

A computer program has been developed to calculate inviscid transonic flow over a swept wing in a wind tunnel with constant rectangular cross sections and with specified normal or tangential flow at the walls. An approximately orthogonal computational grid that conforms to the wing and the tunnel walls was developed for application of the Jameson-Caughey finite-volume algorithm. The code solves the full potential equations in fully conservative form using line relaxation. Sample calculations show the effect of tunnel walls. Comparisons with experimental and other theoretical results are presented.

Introduction

IT is possible to simulate free air flow about a wind tunnel model by controlling inflow and outflow through porous or slotted tunnel walls. The correct normal flow distribution changes with model configuration, angle of attack, and Mach number and is not known a priori. Ferri and Baronti¹ and Sears² have proposed to match the flowfield provided by the tunnel to a computed flowfield beyond the tunnel walls by an iterative adjustment of the boundary conditions at the interface of these two regions.

The Arnold Engineering Development Center is sponsoring a preliminary investigation of this adaptive wall wind tunnel concept to answer questions about plenum compartmentalization required for wall normal flow distribution, sensitivity to pressure measurements, iteration variables, convergence, and other considerations. In order to make this investigation without actually building an adaptive wind tunnel, a computer calculation of the flow in the tunnel will be used, and the computational technique developed for this purpose is described in the following. However, application of the method is not limited to the adaptive wall investigation. The resulting code can be used to assess the severity of wall interference in a conventional tunnel and to correct wind tunnel data. Such an application is particularly important in the transonic regime where conventional wall correction methods fail.

Wind Tunnel Code

The code developed for the tunnel flow solution is based on the finite-volume method of Jameson and Caughey.³ The code solves the full potential equation with nonlinear boundary conditions using fully conservative differencing. One great advantage of this method is that the grid generation scheme can be treated independently from the numerical algorithm. This allows considerable freedom in selecting the grid. Once the grid is generated, the equation solver deals directly with the corner points of the mesh. No analytical mapping of the differential equation is necessary.

Governing Equations and Boundary Conditions

We assume that vorticity generated by shock waves can be ignored so that the velocity (u , v , w) is the gradient of the

potential ϕ ,

$$u = \phi_x, \quad v = \phi_y, \quad w = \phi_z \quad (1)$$

Conservation of mass requires that

$$\frac{\partial}{\partial x}(\rho u) + \frac{\partial}{\partial y}(\rho v) + \frac{\partial}{\partial z}(\rho w) = 0 \quad (2)$$

where the density is given by

$$\rho = \left[1 + \frac{\gamma - 1}{2} M_\infty^2 (1 - q^2) \right]^{1/(\gamma - 1)} \quad (3)$$

$$q^2 = u^2 + v^2 + w^2 \quad (4)$$

Discontinuities in velocity across surfaces are allowed provided the following shock jump conditions apply: 1) continuity of ϕ , implying continuity of the tangential velocity component; 2) continuity of ρu_n , where u_n is the component of velocity normal to the discontinuity surface; and 3) increase of density across the discontinuity surface in the direction of flow.

To obtain the trailing vortex sheet associated with a lifting wing, a discontinuity in ϕ is allowed to occur across a surface trailing downstream from the wing trailing edge. For fixed z (see Fig. 1), the jump in ϕ is maintained constant and equal to the trailing-edge value. This procedure results in a vanishing z component of vorticity in the sheet, a traditional approximation to the required alignment of vorticity with the flow direction. The location of the vortex sheet is not known a priori. The usual procedure of estimating this location and allowing normal flow across the vortex sheet is used. It is required, however, that the normal component of flow be continuous across the sheet.

The conditions to be enforced at the boundaries of the calculation region are now defined. The upstream and downstream boundaries are assumed to be in the far field and thus to have uniform velocity across the wind tunnel with constant cross sections. The upstream value U_∞ is used as the reference velocity, and the downstream value is determined from the tunnel wall boundary conditions, as explained in the following.

Two options are available for boundary conditions on the tunnel wall. The first is the Neumann boundary condition on ϕ which is equivalent to specification of the normal velocity component v_n according to

$$v_n = \frac{\partial \phi}{\partial n} \quad (5)$$

Presented as Paper AIAA 80-0156 at the AIAA 18th Aerospace Sciences Meeting, Pasadena, Calif., Jan. 14-16, 1980; submitted Feb. 5, 1980; revision received Feb. 26, 1981. Copyright © 1981 by John E. Mercer. Published by the American Institute of Aeronautics and Astronautics with permission.

*Senior Research Scientist.

†Research Engineer.

‡Professor, Mechanical and Aerospace Sciences.

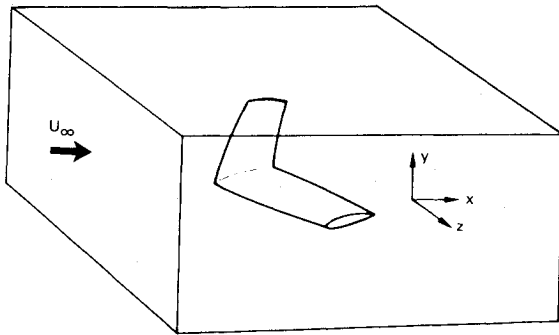


Fig. 1 Cartesian coordinates chosen.

For this wall boundary condition, the downstream boundary condition is required by mass conservation to be

$$\frac{\partial \phi}{\partial x} = U_\infty + \delta u \tag{6}$$

where

$$\delta u = \frac{1}{\rho_d A_d} \int_{\text{tunnel walls}} \rho v_n dS + \left(\frac{\rho_\infty - \rho_d}{\rho_d} \right) U_\infty \tag{7}$$

and where ρ_d is the density at the downstream boundary and A_d the tunnel cross-sectional area at the downstream boundary.

The second option for the tunnel walls is the Dirichlet boundary condition on ϕ which is equivalent to specification of the pressure coefficient C_p at the wall according to the small perturbation relation

$$C_p = -2(u - U_\infty) \tag{8}$$

and

$$\phi = \int_{\text{along wall}} u dx \tag{9}$$

The exact relation between the pressure and the velocity is more complex than that given in Eq. (8). However, for this application, the small perturbation assumption should be sufficient at the wall location, and it provides a convenient simplification. Compatibility with a farfield condition at the downstream boundary requires that the specified u (or C_p) be uniform around the walls at the downstream boundary. The boundary condition on ϕ at the downstream boundary is then

$$\frac{\partial \phi}{\partial x} = u_d = \text{velocity at the tunnel walls at the downstream boundary} \tag{10}$$

Mesh Generation and the Computational Coordinates

One of the principal advantages of the finite-volume method of Jameson and Caughey,³ which was applied to the wind tunnel flow problem at hand, is that transformation to boundary-conforming coordinates is defined by a table of grid points, rather than by mapping functions. Thus, many sequential mapping functions may be used to generate these grid points, but once generated these functions are discarded, and three-dimensional linear interpolation in the transformed space is used when coordinate values are needed at other than grid points. Similarly, scalar fields needed for the numerical calculation (e.g., the velocity potential) are defined by their values at the grid points, and trilinear variation in the transformed space is assumed between grid points.

The mapping from x, y, z Cartesian coordinates to α, β, γ boundary-conforming coordinates for the flow about a swept wing in a wind tunnel with constant cross sections will now be defined. The description involves a number of sequential

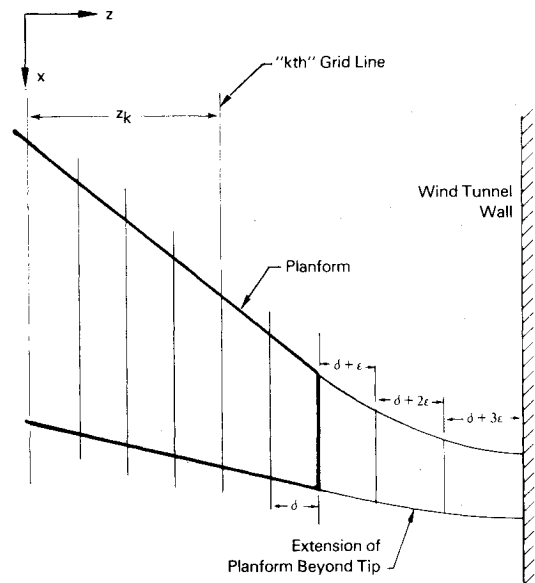
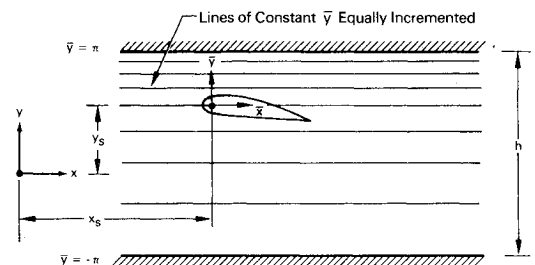


Fig. 2 Z-grid planes and extension of planform for grid generation.



- $\bar{x} = (x - x_s) \times 2\pi/h$
- $\bar{y} = (y - y_s)$
Places Origin of Coordinate System at Reference Point on Airfoil and Scales x According to the Mean y Dimensional Scale
- $\bar{y} = ay' + by'^2$
Moves Model to Center of Tunnel and Scales Dimension so that Tunnel Walls are at $\pm \pi$

Fig. 3 Origin shift, x scaling, and y distortion.

mapping functions. The Cartesian axes are chosen as shown in Fig. 1. The x axis is in the direction of the undisturbed flow and the z axis is in the wing spanwise direction.

Coordinates conforming to the tunnel sidewall are easily obtained by using

$$\gamma = z \tag{11}$$

There remains the task of obtaining an α, β boundary-conforming coordinate system for a physical $x-y$ cut. Since these two-dimensional mappings are partly defined in terms of the airfoil section obtained from the $x-y$ cuts, the wing definition is extended beyond the tip for purposes of grid generation. The planform is extended as shown in Fig. 2, and zero-thickness, flat airfoil sections are assumed. The two-dimensional mapping procedure is similar to that outlined by Caughey and Jameson.⁴ After a shift in origin to the center of curvature of the airfoil nose, and an appropriate scaling in x , a quadratic distortion in y is chosen such that values for the upper and lower tunnel walls are π and $-\pi$, respectively (see Fig. 3). Next, the primary mapping is applied

$$\xi + i\eta = \cosh^{-1} (1 - 2e^{\bar{x} + i\bar{y}}) \tag{12}$$

This mapping allows unwrapping of the domain about an arbitrarily chosen slit line emanating from the origin such that

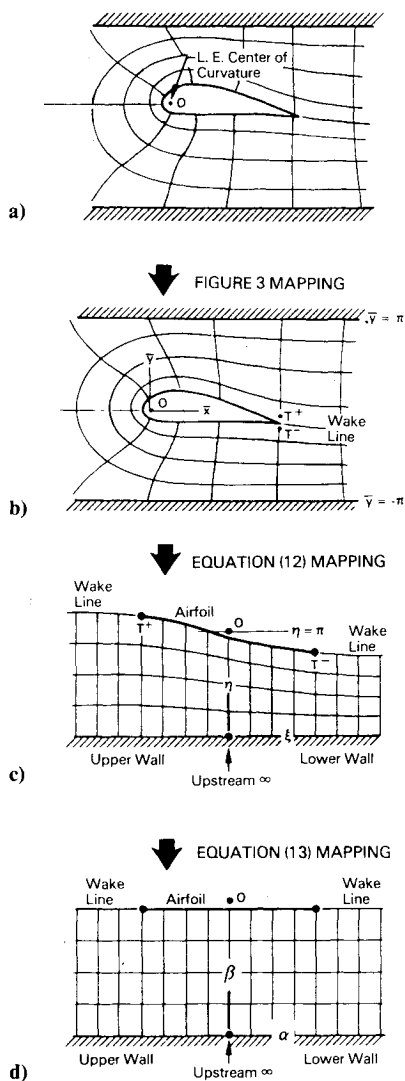


Fig. 4 Sequential mappings from physical to computational space. d) Physical plane (x, y space), b) distorted plane (\bar{x}, \bar{y} space), c) unwrapped plane (ξ, η space), and d) final transformed space (α, β space).

the upper and lower tunnel walls become the lower boundary $\eta = 0$, upstream infinity becomes the origin, and the two sides of the slit plus the airfoil become the upper boundary (located near $\eta = \pi$), as illustrated in Figs. 4b and 4c. The slit line is chosen to pass through the trailing edge, thus eliminating an acute angle on the transformed boundary. It is also convenient to make this slit coincide with the location of the shed vorticity sheet which is assumed to be tangent to the trailing-edge bisector at the trailing edge and parallel to the tunnel wall far downstream. The final transformed coordinates are given by

$$\alpha = \xi, \quad \beta = \eta / \eta_{\text{upper}} \quad (13)$$

where η_{upper} is the value of η along the upper boundary in Fig. 4c. This ordinate stretching gives a coordinate line conforming to the upper boundary.

Having defined a transformation to α, β, γ coordinates which are boundary conforming, we divide the computational region with surfaces of constant α , constant β , and constant γ to form a Cartesian grid in α, β, γ space, as illustrated in Fig. 4d. The increments in α, β , or γ between dividing surfaces need not be equal but must be smooth in order to prevent erroneous numerical results, particularly in the vicinity of shocks. For the γ or z coordinate, the division is made as

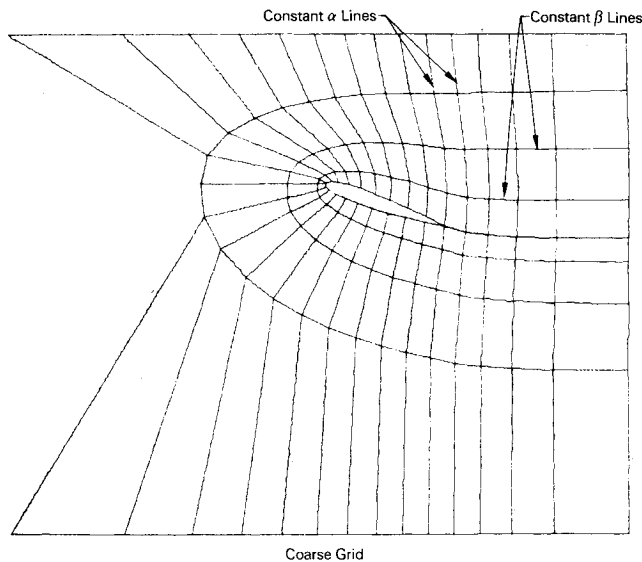


Fig. 5 Computer plot of boundary-conforming coordinates.

shown in Fig. 2. Inboard of the tip, the spacing is uniform; outboard, the spacing is gradually increased or decreased by a small value ϵ per division. For α and β , the spacing is varied to obtain a denser grid near the wing leading edge. An example of the result of these sequential mappings is the computer-generated mesh shown in Fig. 5.

Associated with each six-sided cell into which the transformed space is divided is the set of computational coordinates X, Y, Z used in the next section. To obtain this local coordinate system, the origin is shifted to the center of the cell, and the α, β, γ coordinates are normalized such that there is unit difference between grid points and the vertices of the cubical cell have coordinates

$$X = \pm 1/2, \quad Y = \pm 1/2, \quad Z = \pm 1/2 \quad (14)$$

Tensor notation is used in the remaining discussion where (X, Y, Z) and (x, y, z) are replaced by (X^1, X^2, X^3) and (x^1, x^2, x^3) .

Numerical Method

Details of the finite-volume method are given in Ref. 3. The method is summarized in the following.

The grid in computational space divides the space into cubical cells. This leads to simple difference schemes for the numerical analysis. It can be shown that in terms of quantities associated with computational space, the divergence of the mass flux vector is given by

$$\frac{\partial}{\partial x^i} (\rho u_i) = \frac{\partial}{\partial X^i} (\rho h U^i) \quad (15)$$

where

- u_i = physical velocity components
- U^i = contravariant velocity components
- x^i = physical coordinates
- X^i = transformed coordinates
- h = determinant of the transformation matrix

Also, it can be shown that

$$U^i = g^{ij} \frac{\partial \phi}{\partial X^j} \quad (16)$$

where g^{ij} is the inverse of the metric tensor of the transformation. Thus, to satisfy the governing equation, Eq. (2), the finite-volume algorithm uses an iterative procedure to make the right-hand side of Eq. (15) approach zero.

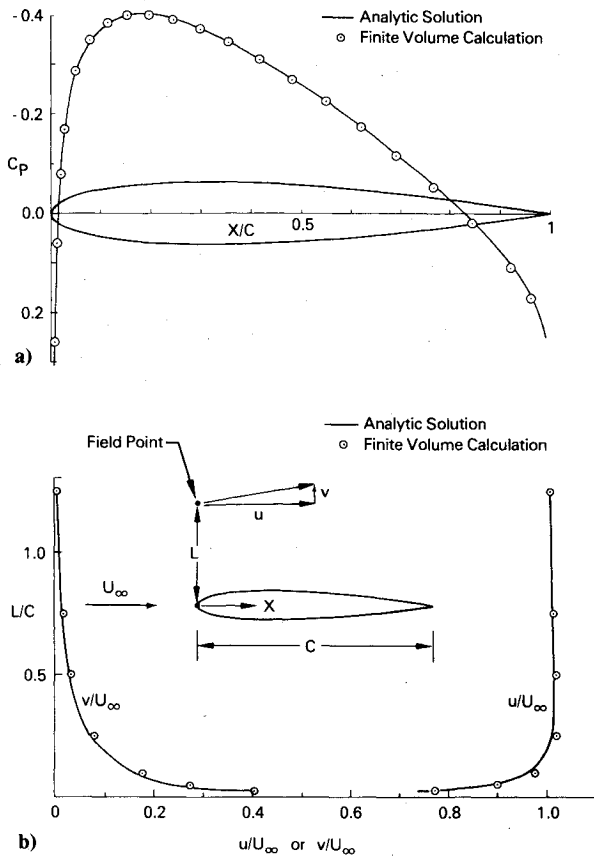


Fig. 6 Incompressible potential flow about a Karman-Trefftz airfoil. a) Surface pressure distribution and b) field point velocities along $x=0$.

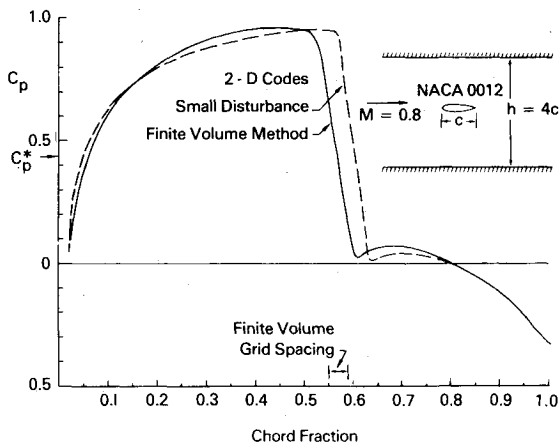


Fig. 7 Calculation of the transonic flow about an NACA 0012 airfoil in the wind tunnel.

The steps for one iteration for the algorithm are listed as follows.

- 1) Using the current values for ϕ , the contravariant velocity U^i is computed using a difference scheme for Eq. (16).
- 2) The density is computed from Eq. (3).
- 3) The divergence of the mass flux vector is computed at each grid point according to Eq. (15) using a box difference scheme on a set of secondary cells nested in the primary set.
- 4) Additional terms are added to the divergence to obtain an artificial viscosity, to offset certain lumping errors, and to embed the steady-state equation in a convergent time-dependent process (the iteration) which evolves to the solution (see Ref. 3 for details).
- 5) New grid point values for ϕ are calculated to reduce the divergence to zero using successive line over-relaxation.

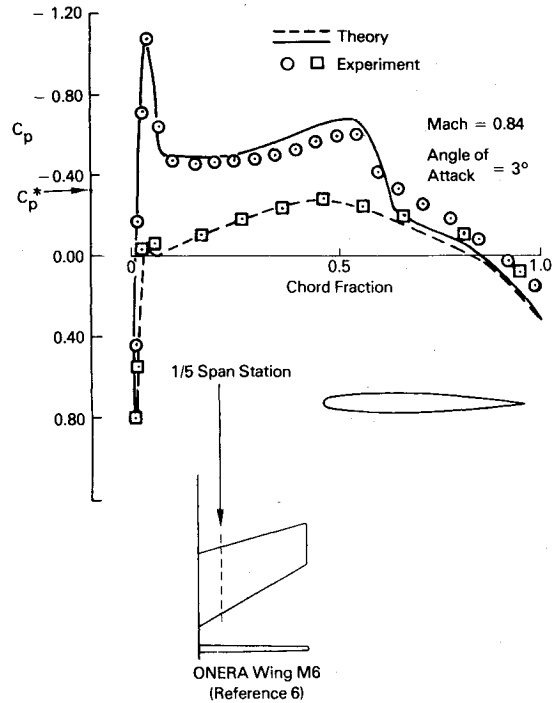


Fig. 8 Finite-volume calculation and wind tunnel results for transonic flow about a swept wing in free air.

For more efficient calculation, three grid sizes are used in sequence.

Initially, a converged solution is obtained for a coarse grid, as exemplified in Fig. 5. This solution is used to initialize the calculation for a medium grid which is obtained from the coarse grid by halving the spacing. After iterating to a converged solution on the medium grid, refinement is carried one step further using a fine grid obtained by halving the medium grid.

The numerical solution initially gives the values of ϕ at the grid points. The velocity is then calculated as follows. Since gradients are easily evaluated in the computational plane, Eq. (1) is first reformulated using the chain rule to obtain

$$u_i = \frac{\partial X^j}{\partial x^i} \frac{\partial \phi}{\partial X^j} \quad (17)$$

The grid point values of the velocity are calculated according to Eq. (17) by central differencing and are interpolated linearly in computational space to obtain the velocity at any point desired.

Example Calculations and Code Validation

Various sample calculations are presented, including those made for comparison with experimental and other theoretical results. All of the comparisons with experimental data are for cases with insignificant wall effects. No three-dimensional experimental results with significant wall effects and known wall boundary conditions were located. The ability of the code to treat properly the tunnel wall boundary condition was checked out using the results of other theoretical methods. These methods are two dimensional, so the code calculations for these comparisons were made with unswept wings spanning the tunnel.

Comparison with an exact incompressible potential flow calculation is presented in Fig. 6 for a Karman-Trefftz airfoil in a tunnel. The exact solution was obtained by calculating the free air flow about the airfoil using analytical procedures. The normal component of velocity was calculated along a line parallel to the freestream and above the airfoil as the upper tunnel wall boundary condition for the finite-volume method

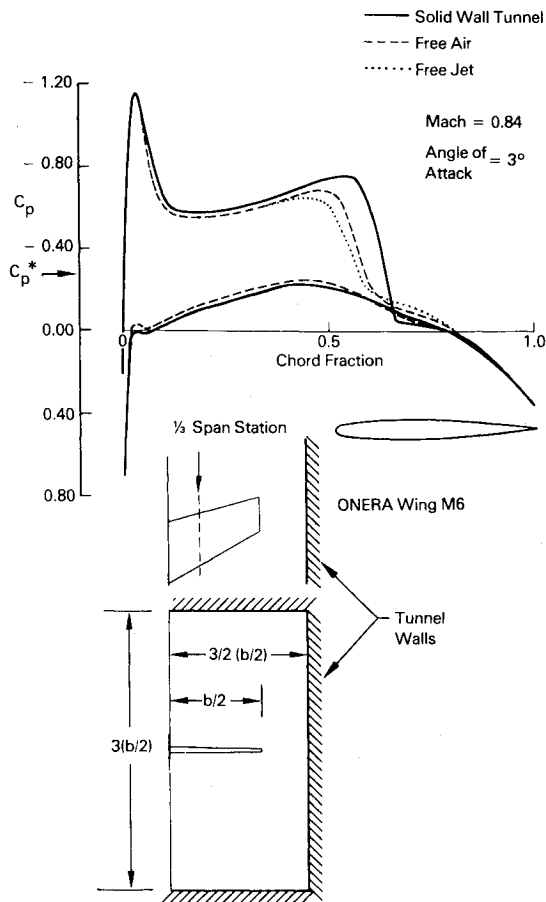


Fig. 9 Comparison of calculations for free air, free jet and solid tunnel wall conditions.

computer calculation and similarly for the lower wall. The agreement at the airfoil surface and at the field points given in Fig. 6 is excellent. Field point comparison along a line going to the leading edge was chosen to illustrate the accuracy of the calculations where the errors would be most noticeable. Maximum discretization error for the finite-volume method is expected near the leading edge where velocity gradients are largest. This comparison provides a validation for proper treatment of wall boundary conditions and for calculation of field point velocities.

To provide a transonic check case with tunnel walls, the two-dimensional flow about a NACA 0012 airfoil at a Mach number of 0.8 with solid tunnel walls (no normal flow) four chord lengths apart was calculated. Figure 7 shows a comparison with the small disturbance method described by Murman et al.⁵ Here again the agreement is quite good. The

pressure levels are very close, and it is expected that a full potential equation solution will give a shock position upstream of the small disturbance equation solution.

Three-dimensional transonic calculations were made for the ONERA Wing M6 for free air conditions. In Fig. 8, these calculations are compared with experimental data for a slotted wall tunnel that was approximating free-air conditions.⁶ The calculation was repeated with tunnel wall boundary conditions enforced. Both zero normal velocity (the solid wall condition) and zero tangential velocity perturbation [approximately the free jet condition according to Eq. (8)] were enforced. The results, shown in Fig. 9, display the expected shift in upper surface pressure level and shock position.

Summary

A computer code for a wing in a transonic wind tunnel has been developed which can enforce normal and tangential flow boundary conditions at the wall. The output from the code provides pressures, velocities, and local Mach numbers on the wing and at any points in the flowfield specified by the user. Validation of the code is indicated by the favorable comparisons with the results of other numerical and analytical methods. Comparisons with wind tunnel data have been limited to cases with insignificant wall effects because of a lack of appropriate data. Expected effects were obtained from calculations with tunnel wall boundary conditions enforced.

Acknowledgment

This work was sponsored by the Arnold Engineering Development Center under Contract F40600-79-C-001, "Development of a Computer Code to Model Three-Dimensional Self-Correcting Transonic Wind Tunnels."

References

- ¹Ferri, A. and Baronti, P., "A Method for Transonic Wind Tunnel Corrections," *AIAA Journal*, Vol. 11, Jan. 1973, pp. 63-66.
- ²Sears, W. R., "Self-Correcting Wind Tunnels," *Aeronautical Journal*, Vol. 78, Feb./March 1974, pp. 80-89.
- ³Jameson, A. and Caughey, D. A., "A Finite-Volume Method for Transonic Potential Flow Calculations," *Proceedings of AIAA 3rd Computational Fluid Dynamics Conference*, Albuquerque, N. Mex., June 27-28, 1977, pp. 35-54.
- ⁴Caughey, D. A. and Jameson, A., "Numerical Calculation of Transonic Potential Flow about Wing-Body Combinations," *AIAA Journal*, Vol. 17, Feb. 1979, pp. 175-181.
- ⁵Murman, E. M., Bailey, F. R., and Johnson, M. H., "TSFOIL—A Computer Code for 2-D Transonic Calculations, Including Wind-Tunnel Wall Effects and Wave-Drag Evaluation," NASA SP-347, Pt. II, 1975, pp. 769-788.
- ⁶Monnerie, B. and Charpin, F., "Essais de buffeting d'une aile en flèche en transsonique," *10^e Colloque d'Aérodynamique Appliqué*, Lille, Nov. 1973.